Suplemento de la Revista Mexicana de Física **4** 021112 (2023) 1–5

Speed of sound of a non-equilibrium medium formed at LHC energies

J. R. Alvarado García, I. Bautista, and A. Fernández Téllez

Facultad de Ciencias Físico Matemáticas, Benemérita Universidad Autónoma de Puebla,
1152, Puebla 72570, México.
e-mail: j.ricardo.alvarado@cern.ch

Received 14 May 2023; accepted 22 June 2023

We estimate the squared speed of sound for the hot and dense QCD states formed in ion collisions at very high energies by exploring the implications of small-bounded and geometry effects in the Color String Percolation Model. The squared sound velocity shows signals of a local minimum (knee point) below the critical temperature consistent with the softest point in the equation of state and the onset of quark deconfinement that characterizes the quark-gluon plasma phase transition.

Keywords: Speed of sound; sound velocity; quark-gluon plasma; heavy ions; percolation.

DOI: https://doi.org/10.31349/SuplRevMexFis.4.021112

1. Introduction

A successful way to characterize the properties of quark-gluon plasma (QGP) is to use the relativistic dissipative hydrodynamics formalism [1–3]. In which one of the most important quantities appears, the speed of sound c_s [4]. This thermodynamic observable carries important information in describing the evolution of the fireball in heavy ion collisions and is a measurement of particle density and mean free path.

The speed of sound is especially important in the study of QCD phase transition given that its value affects the dynamics of density perturbations making it a fundamental property of strongly interacting matter. Many attempts in estimating the c_s^2 value in QCD matter have been performed in LQCD [5–9], (P)NJL model [2, 10, 11], quark-meson coupling model [12, 13], hadron resonance gas (HRG) model [14, 15], field correlator method (FCM) [16, 17] , quasiparticle model [18], and is usually extracted from the width of Gaussian rapidity distribution data described by the Landau hydrodynamic model [19–22].

In this work, we estimate the c_s^2 dependence with temperature in the framework of the Color String Percolation Model (CSPM) by introducing small-bounded effects leading to a relevant deviation from the thermodynamic limit (TL). The content of the manuscript is organized by the following: In Sec. 2, we introduce the basics of CSPM, explaining the effects of clustering formation and we purpose a parameterization that considers small-bounded effects introduced in the percolating system. In Sec. 3 we establish the formulation of thermodynamic observables in the framework of the CSPM. The formulation of c_s^2 is given in Sec. 4 and, finally, we discuss the results of this work in Sec. 5.

2. Color string percolation model

In the picture of the CSPM, the interaction between colliding nucleons is represented by the formation of extended color flux tubes (Lund model-like strings [23]) which are stretching among the colliding partons and carry a fraction of the partons momentum, as pictorially illustrated in Fig. 1.

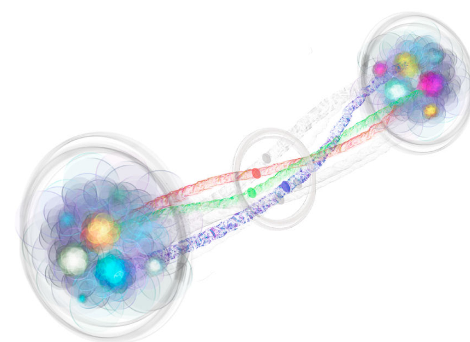

FIGURE 1. Sketch of two colliding protons where a set of color flux tubes is formed representing the interaction between partons.

The color flux tubes project their transversal areas into an interaction area over the impact parameter plane, the transverse strings formed are represented by fully penetrable disks (as seen in Fig. 1), and we estimate the effective projection area of disks from the parton-parton cross section ~ 3.5 mb [24].

The collective phenomena are studied from the 2-dimensional continuum percolation theory applied to color strings, which can overlap each other giving rise to different regions called color sources.

As seen in Fig. 2, a certain number of strings N created in the collision event with area S_0 are distributed over the total interaction area S. For characterizing the system we use the filling factor which depends on the area fraction occupied by a determined number of strings over the transverse plane [25]:

$$\xi = NS_0/S. \tag{1}$$

The number of initial strings depends on the nucleon number, multiplicity, and energy of the colliding system. The

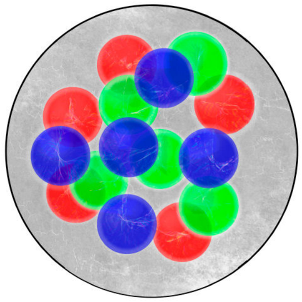

FIGURE 2. Scheme of ($N = 15$) transverse color strings over interacting (gray) area S.

growth of the strings' number allows the formation of a spanning cluster marking a geometric phase transition in the context of percolation theory.

The vectorial sum of the color fields on each color source contributes to the cluster giving a decrease in multiplicity μ_0 produced by N single strings [25–27]:

$$\mu = \mu_0 F(\xi) N. \tag{2}$$

The multiplicity is damped by an emerging functional scaling from the clustering formation $F(\xi)$, the so-called Color Reduction Factor [28]. This function increases with the string tension of the cluster and the average momentum fraction of the partons $\langle p_T^2 \rangle = \langle p_T^2 \rangle_0 / F(\xi)$.

In the thermodynamic limit, $F(\xi)$ depends on ξ distribution as $F(\xi) = \sqrt{(1 - e^{-\xi})/\xi}$ [25].

The recent Monte Carlo results that took into account the correction with size, initial geometry of the overlapping area, and profile distribution function [29,30] are taken for parameterize the largest deviation from the TL behavior by introducing a modification on the $F(\xi)$ adding an additional damping term:

$$F_s(\xi) = F(\xi)(m + c\sqrt{\text{coth}(\xi/2)}), \tag{3}$$

where $m = 0.7714731 \pm 0.01468$ is a weight parameter of the TL contribution to $F(\xi)$, and $c = 0.0609589 \pm 0.007527$ is the corresponding weight parameter of the deviation from the usual conditions considered in the percolating system.

3. Thermodynamic observables

The CSPM has described successfully the collective effects on heavy ion collision's medium formed at RHIC and LHC energies through the estimation of certain observables [25, 26, 31–37]. In the following, we introduce some of the necessary thermodynamic quantities that can be obtained in the framework of this model.

3.1. Thermal distribution

Thermal distribution involves the Schwinger mechanism for non-massive particles and is given by a p_T squared exponential. Color interactions cause the string tension to fluctuate around its mean value $\langle x^2 \rangle$ described by a Gaussian distribution that gives rise to a thermal distribution characterized by the mean transverse momentum of a single string $\langle p_T^2 \rangle_0 = \langle x^2 \rangle F_s(\xi)/\pi$ [25,38]:

$$\frac{dN}{dp_T^2} \sim \exp\left(-p_T\sqrt{\frac{2F_s(\xi)}{\langle p_T^2 \rangle_0}}\right), \tag{4}$$

from where we obtain an estimated temperature:

$$T(\xi) = \sqrt{\frac{\langle p_T^2 \rangle_0}{2F_s(\xi)}}. \tag{5}$$

We consider the critical temperature in terms of the percolation threshold, which is defined as the critical string density ξ_c. It is important to mention that $F_s(\xi)$ requires the corresponding ξ_{sc} to be determined not in the thermodynamic limit. The value of ξ_{sc} falls between 0.5 and 0.72 [29] and $F_s(\xi_{sc})$ is very close to $F(\xi_c)$, where $\xi_c \sim$ 1.128 is the percolation threshold in TL [39]. Therefore, we have chosen to compare the results using $F(\xi_c)$ by considering $T_c = T(\xi c)$, that is $T/T_c = 0.87995/\sqrt{F_s(\xi)}$.

With this choice, we observe a shift in the critical temperature compared to what has been previously reported in the thermodynamic limit [25,26]. It is now reached at $\xi \sim 0.571$ for $F_s(\xi)$. For the subsequent calculations, we consider the critical temperature $T_c = 154 \pm 9$ as reported in Ref. [40].

3.2. Energy density

The energy density ε scales with the number of degrees of freedom "observed" in the medium, and its rapid growth marks the phase transition from Hadron Gas (HG) to QGP.

It was found that exist a direct relation between string density ξ and energy density ε, given that ξ is the local order parameter in the CSPM geometric phase transition [25]. The energy density from the Bjorken boost invariant 1D hydrodynamics formula [41] is found to be proportional to ξ [25,42,43]. So, we use the relation $\varepsilon = \varsigma\xi$ to estimate energy density, with $\varsigma = 0.5601$ GeV/fm^3.

The values of the critical energy density ε_c, corresponding to $\varepsilon(T_c)$ are in between 0.5558 GeV/fm^3 and 0.7638 GeV/fm^3.

3.3. Equation of state

Trace anomaly Δ measures the deviation with respect to the conformal behavior identifying residual interactions in the medium formed [44–46], its value makes the connection between quantum field theory phenomena and medium properties. This observable is closely related to the medium's transport coefficients. It has been observed qualitatively that the trace anomaly can be approximated as the inverse of shear viscosity over entropy density [47, 48], The shear viscosity to entropy density ratio is defined in the context of kinetic theory as $\eta/s = \lambda T/5$, whit λ the mean free path

$\sim 1/(\tilde{n}\sigma_{tr})$ where $\tilde{n} \sim nF_s(\xi)/(LS)$ is the density number and $\sigma_{tr} \sim F_s(\xi)S_0$ the transport cross section [49]. By using Eq. (1):

$$\frac{\eta}{s} = \frac{TL}{5\xi F_s^2(\xi)}, \tag{6}$$

with $L \sim 1$ fm the longitudinal extension of color strings.

The trace anomaly gives us the first step to construct a relation between the pressure P, and energy density through the relation $T^4\Delta = \varepsilon - 3P$ [47,48]:

$$\frac{\varepsilon - 3P}{T^4} \sim \frac{5\xi F_s^2(\xi)}{TL}. \tag{7}$$

Finally, we use the relation at vanishing chemical potential $Ts = P + \varepsilon$ in order to introduce the entropy density [41].

4. Speed of sound

The first harmonic flow components of the system are non-neglectable due to the non-zero effect of bulk viscous pressure which affects the energy density profile converting it into pressure gradients measured by the speed of sound c_s^2 [43]. This effect is related to the small perturbations in the medium [43] and by using a known thermodynamic relation which can be expressed in terms of CSPM observables [41]:

$$c_s^2 = \left(\frac{\partial P}{\partial \varepsilon}\right)_s = s\left(\frac{\partial T}{\partial \varepsilon}\right)_s = -\frac{sT}{2\varsigma F_s} \cdot \frac{dF_s}{d\xi}. \tag{8}$$

In Fig. 3, we plot the dependence of c_s^2 with T/T_c. It is important to mention that the use of $F_s(\xi)$ exhibits a different behavior compared to what was previously reported [25,35,36,43]. Specifically, a large deviation from TL is observed in the region below the critical temperature, displaying a "dip-and-bump" effect. This behavior is in agreement with other phenomenological models [11] and is consistent with findings reported from LatticeQCD simulations using the 2+1 flavor staggered fermion actions p4 and asqtad [42], as well as the highly improved staggered quark action from the HotQCD Collaboration [6].

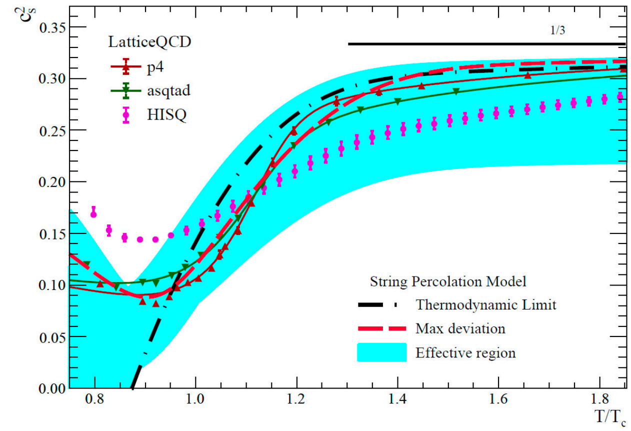

FIGURE 3. Dependence of c_s^2 with T/T_c calculated in the CSPM framework using Eq. (8), the effective estimate region (cyan area), our parameterization (red dashed line) and thermodynamic limit (black dotted-dashed line) are shown. The magenta circles are the HISQ action extrapolated results from the HotQCD Collaboration [6]. Meanwhile, the maroon and green triangles correspond to p4 and asqtad staggered fermion actions respectively, with their respective parameterization in continuum lines [**?**].

5. Conclusions

We have introduced a modification to the CSPM through one of its main parameters allowing a better description of the bulk properties and transport coefficients of non-equilibrium systems. Our results of thermodynamic quantities values, specifically the speed of sound, are in agreement with the LQCD predictions.

With this new perspective, we can extend the application of CSPM to describe the experimental data from pp to AA collisions at very high energies.

1. H. Song, *et al.*, 200 A GeV Au+Au collisions serve a nearly perfect quark-gluon liquid, *Phys. Rev. Lett.* **106** (2011) 192301, `https://doi.org/10.1103/PhysRevLett.106.192301`.
2. H. Song, S. A. Bass, and U. Heinz, Viscous QCD matter in a hybrid hydrodynamic+Boltzmann approach, *Phys. Rev. C* **83** (2011) 024912, `https://doi.org/10.1103/PhysRevC.83.024912`.
3. P. Deb, G. P. Kadam, and H. Mishra, Estimating transport coefficients in hot and dense quark matter, *Phys. Rev. D* **94** (2016) 094002, `https://doi.org/10.1103/PhysRevD.94.094002`.
4. M. Albright and J. I. Kapusta, Quasiparticle Theory of Transport Coefficients for Hadronic Matter at Finite Temperature and Baryon Density, *Phys. Rev. C* **93** (2016) 014903, `https://doi.org/10.1103/PhysRevC.93.014903`.
5. Y. Aoki, *et al.*, The Order of the quantum chromodynamics transition predicted by the standard model of particle physics, *Nature* **443** (2006) 675, `https://doi.org/10.1038/nature05120`.
6. A. Bazavov *et al.*, Equation of state in (2+1)-flavor QCD, *Phys. Rev. D* **90** (2014) 094503, `https://doi.org/10.1103/PhysRevD.90.094503`.
7. S. Borsányi, *et al.*, Full result for the QCD equation of state with 2+1 flavors, *Phys. Lett. B* **730** (2014) 99, `https://doi.org/10.1016/j.physletb.2014.01.007`.
8. S. Borsanyi, *et al.*, QCD Crossover at Finite Chemical Potential from Lattice Simulations, *Phys. Rev. Lett.* **125** (2020) 052001, `https://doi.org/10.1103/PhysRevLett.125.052001`.

9. O. Philipsen, The QCD equation of state from the lattice, *Prog. Part. Nucl. Phys*. **70** (2013) 55, https://doi.org/10.1016/j.ppnp.2012.09.003.
10. M. Motta, *et al*., Isentropic evolution of the matter in heavy-ion collisions and the search for the critical endpoint, *Eur. Phys. J. C* **80** (2020) 770, https://doi.org/10.1140/epjc/s10052-020-8218-x.
11. W.-b. He, *et al*., Speed of sound in QCD matter, *Phys. Rev. D* **105** (2022) 094024, https://doi.org/10.1103/PhysRevD.105.094024.
12. B.-J. Schaefer, M. Wagner, and J. Wambach, Thermodynamics of (2+1)-flavor QCD: Confronting Models with Lattice Studies, *Phys. Rev. D* **81** (2010) 074013, https://doi.org/10.1103/PhysRevD.81.074013.
13. A. Abhishek, H. Mishra, and S. Ghosh, Transport coefficients in the Polyakov quark meson coupling model: A relaxation time approximation, *Phys. Rev. D* **97** (2018) 014005, https://doi.org/10.1103/PhysRevD.97.014005.
14. R. Venugopalan and M. Prakash, Thermal properties of interacting hadrons, *Nucl. Phys. A* **546** (1992) 718, https://doi.org/10.1016/0375-9474(92)90005-5.
15. M. Bluhm, *et al*., Lattice QCD-based equations of state at vanishing net-baryon density, *Nucl. Phys. A* **929** (2014) 157, https://doi.org/10.1016/j.nuclphysa.2014.06.013.
16. Z. V. Khaidukov, M. S. Lukashov, and Y. A. Simonov, Speed of sound in the QGP and an SU(3) Yang-Mills theory, *Phys. Rev. D* **98** (2018) 074031, https://doi.org/10.1103/PhysRevD.98.074031.
17. Z. V. Khaidukov and Y. A. Simonov, Thermodynamics of a quark-gluon plasma at finite baryon density, *Phys. Rev. D* **100** (2019) 076009, https://doi.org/10.1103/PhysRevD.100.076009.
18. V. Mykhaylova and C. Sasaki, Impact of quark quasiparticles on transport coefficients in hot QCD, *Phys. Rev. D* **103** (2021) 014007, https://doi.org/10.1103/PhysRevD.103.014007.
19. D. ter Haar, ed., Collected Papers of L.D. Landau (Pergamon, 1965), https://doi.org/10.1016/c2013-0-01806-3.
20. C.-Y. Wong, Landau Hydrodynamics Revisited, *Phys. Rev. C* **78** (2008) 054902, https://link.aps.org/doi/10.1103/PhysRevC.78.054902.
21. Z. Jian, *et al.*, Unified Descriptions of Hwa-Bjorken and Landau Relativistic Hydrodynamics and the Pseudorapidity Distributions in High Energy Heavy Ion Collisions, *Nucl. Phys. Rev.* **32** (2015) 398, https://www.npr.ac.cn/en/article/doi/10.11804/NuclPhysRev.32.04.398.
22. A. M. Kamchatnov, Landau-Khalatnikov Problem in Relativistic Fluid Dynamics, *J. Exp. Theor. Phys*. **129** (2019) 607, https://doi.org/10.1134/S1063776119100200.
23. B. Andersson, *et al*., Parton Fragmentation and String Dynamics, *Phys. Rept.* **97** (1983) 31, https://doi.org/10.1016/0370-1573(83)90080-7.
24. N. S. Amelin, M. A. Braun, and C. Pajares, Multiple production in the Monte Carlo string fusion model, *Phys. Lett. B* **306** (1993) 312, https://doi.org/10.1016/0370-2693(93)90085-V.
25. M. A. Braun, *et al.*, De-Confinement and Clustering of Color Sources in Nuclear Collisions, *Phys. Rept.* **599** (2015) 1, https://doi.org/10.1016/j.physrep.2015.09.003.
26. M. A. Braun and C. Pajares, Implications of percolation of color strings on multiplicities, correlations and the transverse momentum, *Eur. Phys. J. C* **16** (2000) 349, https://doi.org/10.1007/s100520050027.
27. I. Bautista, C. Pajares, and J. E. Ramírez, String percolation in AA and p+p collisions, *Rev. Mex. Fis*. **65** (2019) 197, https://doi.org/10.31349/RevMexFis.65.197.
28. I. Bautista, A. F. Téllez, and P. Ghosh, Indication of change of phase in high-multiplicity proton-proton events at LHC in String Percolation Model, *Phys. Rev. D* **92** (2015) 071504, https://doi.org/10.1103/PhysRevD.92.071504.
29. J. E. Ramírez, A. Fernández Téllez, and I. Bautista, String percolation threshold for elliptically bounded systems, *Physica A* **488** (2017) 8, https://doi.org/10.1016/j.physa.2017.07.002.
30. J. E. Ramírez and C. Pajares, Area covered by disks in smallbounded continuum percolating systems: An application to the string percolation model, *Phys. Rev. E* **100** (2019) 022123, https://doi.org/10.1103/PhysRevE.100.022123.
31. I. Bautista, J. D. de Deus, and C. Pajares, Elliptic flow at RHIC and LHC in the string percolation approach, *Eur. Phys. J. C* **72** (2012) 2038, https://doi.org/10.1140/epjc/s10052-012-2038-6.
32. I. Bautista, *et al*., Rapidity dependence of particle densities in pp and AA collisions, *Phys. Rev. C* **86** (2012) 034909, https://doi.org/10.1103/PhysRevC.86.034909.
33. I. Bautista, J. Dias de Deus, and C. Pajares, String percolation and the first LHC data, *Acta Phys. Polon. Supp.* **6** (2013) 165, https://doi.org/10.5506/APhysPolBSupp.6.165.
34. C. Andrés, M. Braun, and C. Pajares, Energy loss as the origin of a universal scaling law of the elliptic flow, *Eur. Phys. J. A* **53** (2017) 41, https://doi.org/10.1140/epja/i2017-12226-5.
35. B. K. Srivastava, Percolation and Deconfinement, *Nucl. Phys. A* **862-863** (2011) 132, https://doi.org/10.1016/j.nuclphysa.2011.05.031.
36. R. P. Scharenberg, B. K. Srivastava, and A. S. Hirsch, Percolation of Color Sources and the determination of the Equation of State of the Quark-Gluon Plasma (QGP) produced in central Au-Au collisions at $\sqrt{SNN}$ = 200-GeV, *Eur. Phys. J. C* **71** (2011) 1510, https://doi.org/10.1140/epjc/s10052-010-1510-4.
37. J. E. Ramírez, B. Díaz, and C. Pajares, Interacting color strings as the origin of the liquid behavior of the quark-gluon plasma, *Phys. Rev. D* **103** (2021) 094029, https://doi.org/10.1103/PhysRevD.103.094029.

38. A. Bialas, Fluctuations of string tension and transverse mass distribution, *Phys. Lett. B* **466** (1999) 301, https://doi.org/10.1016/S0370-2693(99)01159-4.

39. S. Mertens and C. Moore, Continuum percolation thresholds in two dimensions, *Phys. Rev. E* **86** (2012) 061109, https://doi.org/10.1103/PhysRevE.86.061109.

40. A. Bazavov *et al*., The chiral and deconfinement aspects of the QCD transition, *Phys. Rev. D* **85** (2012) 054503, https://doi.org/10.1103/PhysRevD.85.054503.

41. J. D. Bjorken, Highly Relativistic Nucleus-Nucleus Collisions: The Central Rapidity Region, *Phys. Rev. D* **27** (1983) 140, https://doi.org/10.1103/PhysRevD.27.140.

42. J. Dias de Deus, *et al*., Clustering of color sources and the shear viscosity of the QGP in heavy ion collisions at RHIC and LHC energies, *Eur. Phys. J. C* **72** (2012) 2123, https://doi.org/10.1140/epjc/s10052-012-2123-x.

43. P. Sahoo, *et al.*, Thermodynamic and transport properties in Au + Au collisions at RHIC energies from the clustering of color strings, *Mod. Phys. Lett. A* **34** (2019) 1950034, https://doi.org/10.1142/S0217732319500342.

44. A. D. Gasbarro, Studies of Conformal Behavior in Strongly Interacting Quantum Field Theories, Ph.D. thesis, Yale U. (2019).

45. K. I. Ishikawa, *et al.*, Conformal Behavior in QCD (2013).

46. M. Cheng *et al.*, Equation of State for physical quark masses, *Phys. Rev. D* **81** (2010) 054504, https://doi.org/10.1103/PhysRevD.81.054504.

47. B. K. Srivastava, Percolation Approach to Initial Stage Effects in High Energy Collisions, *Nucl. Phys. A* **926** (2014) 142, https://doi.org/10.1016/j.nuclphysa.2014.04.029.

48. J. Dias de Deus *et al*., Transport Coefficient to Trace Anomaly in the Clustering of Color Sources Approach, *Phys. Rev. C* **93** (2016) 024915, https://doi.org/10.1103/PhysRevC93.024915.

49. A. Bazavov *et al*., Equation of state and QCD transition at finite temperature, *Phys. Rev. D* **80** (2009) 014504, https://doi.org/10.1103/PhysRevD.80.014504.